Materials Science and Engineering C 55 (2015) 579–591

Contents lists available at ScienceDirect

Materials Science and Engineering C

journal homepage: www.elsevier.com/locate/msec

Investigations on the performance of poly(o-anisidine)/graphene nanocomposites for the electrochemical detection of NADH

D. Sangamithirai [a], V. Narayanan [b], B. Muthuraaman [c], A. Stephen [a,*]

[a] Department of Nuclear Physics, University of Madras, Guindy Campus, Chennai 600025, India
[b] Department of Inorganic Chemistry, University of Madras, Guindy Campus, Chennai 600025, India
[c] Department of Energy, University of Madras, Guindy Campus, Chennai 600025, India

ARTICLE INFO

Article history:
Received 23 January 2015
Received in revised form 15 April 2015
Accepted 25 May 2015
Available online 30 May 2015

Keywords:
Poly(o-anisidine)
Graphene
Nanofibers
Electrochemical sensor
NADH

ABSTRACT

The electrocatalytic oxidation of dihydronicotinamide adenine dinucleotide (NADH) based on poly(o-anisidine)/graphene (POA/GR) nanocomposites modified glassy carbon electrode (GCE) was explored for the first time. POA/GR nanocomposites were synthesized via chemical oxidative polymerization method. X-ray diffraction (XRD), field emission scanning electron microscopy (FESEM), high resolution transmission electron microscopy (HRTEM), Fourier transform infrared spectroscopy (FTIR), Raman spectroscopy, and UV–Vis spectroscopy results demonstrate that nanocomposites are successfully synthesized. An intriguing composite structure was observed using different ratios of o-anisidine monomer and graphene. The electrical properties and electrochemical properties of these nanocomposites are investigated by impedance spectroscopy technique and cyclic voltammetric (CV) method, respectively. The synthesized nanocomposites were used to modify glassy carbon electrode (GCE), and the modified electrodes were found to exhibit electrocatalytic activity for oxidation of NADH at low potential range of +0.045 V in a neutral environment. The fabricated sensor based on POA/GR31-modified GCE exhibited enhanced current response with very high sensitivity of 47.1 μA μM^{-1} for the detection of NADH. The developed POA/GR-modified GCE exhibited excellent reproducibility, stability, and selectivity for the determination of NADH. The practical analytical utility of the proposed method was demonstrated by NADH spiked ascorbic acid (AA) and the results confirmed that the proposed method is suitable for the determination of NADH in the presence of AA. This can open up new opportunities for simple and selective detection of NADH and provide a promising platform for biosensor designs.

1. Introduction

NADH is an important coenzyme produced in vivo during dehydrogenase based enzymatic reactions and it has a number of essential roles in biological systems [1]. It acts as a coenzyme in redox reactions, as a donor of adenosine diphosphate (ADP)-ribose moieties in ADP-ribosylation reactions, as a precursor of the second messenger molecule cyclic ADP-ribose, as well as acting as a substrate for bacterial DNA ligases and a group of enzymes called sirtuins that use NAD^+ to remove acetyl groups from proteins. In addition to these metabolic functions, NAD^+ emerges as an adenine nucleotide that can be released from cells spontaneously and by regulated mechanisms [2] and can so have important extracellular roles [3]. The electrochemical oxidation of NADH has attracted considerable attention due to its importance both as a cofactor for dehydrogenase enzymes and its role in the electron-transfer chain in biological system [4]. Therefore, researches on the electrochemical oxidation of NADH have drawn considerable attention [5]. However, direct oxidation of NADH at bare electrode occurs at a high over potential (>1.0 V) and suffers from low sensitivity and the fouling of the electrode surface by its oxidation products, which causes loss of selectivity, reproducibility and stability [6,7]. In recent years, many nanomaterials, such as poly(1,2-diaminobenzene), polyaniline, TiO_2, carbon nanotubes (CNTs), carbon nanofibers and graphene have been devoted to decrease the high overpotential for NADH electro-oxidation and minimize the surface fouling to meet the need of rapid development of dehydrogenase-based bioelectrochemical devices [8–13].

As a new class of electrode materials, conducting polymers provide a suitable platform for the detection of biological analytes [14]. Conducting polymers have been used as potential systems for the immobilisation of enzymes due to their numerous compelling features such as (i) the ability to transfer the electrons directly to and from the enzymes and simultaneously act as suitable matrices for entrapment of the enzymes; (ii) the conducting polymers exhibit flexible chemical structure; (iii) these materials are compatible with neutral solutions which is essential for enzyme activity and (iv) good stability in aqueous solutions and air [15,16]. Polyaniline (PANI), as one of the most important conducting polymers had been extensively investigated because of its good electronic and

* Corresponding author.
E-mail address: stephen_arum@hotmail.com (A. Stephen).

http://dx.doi.org/10.1016/j.msec.2015.05.066
0928-4931/

optical properties, ease of synthesis, and good environmental stability [17–19]. In the case of sensor applications, nanostructured PANI has great sensitivity and fast response time due to its highly effective surface area and short penetration depth for target molecules [20]. However, pure PANI is electroactive only when the pH is under 4.0 [21,22]. This is an obstacle to its application in sensor which normally requires a neutral environment. Interestingly, Luo et al. reported that carbon nanotubes (CNTs) can enhance the stability of their PANI based biosensor by effectively adsorbing the enzymes present in the reaction and also by increasing the electron transfer between the electrode and the enzyme. Additionally, Liu et al. has paved a way to shift the conductive property of PANI to a neutral pH by constructing PANI/CNT layers through layer-by-layer assembly, which was reported to be very stable and capable of detecting NADH at a very low potential [23]. On the basis of these reports, functionalization of PANI with CNTs, fullerenes and graphene provides a new class of carbon-based advanced materials for sensor applications [24]. Graphene (GR), a two-dimensional and single layer sheet of sp^2 hybridized carbon atoms, has attracted a great deal of attention from both the experimental and theoretical scientific communities in the past several years [25]. Conducting polymer composites containing graphene possess good electrical conductivity and mechanical stiffness [26]. Several reports have been made on incorporating graphene into polymer matrices to produce novel nanocomposite materials. It was found that a homogeneously dispersed graphene nanofiller in a polymer matrix provided nanocomposites with enhanced mechanical, electrical, thermal, and other properties due to the large surface-to-volume ratios of the nanofiller [27,28]. Many groups have reported on the synthesis of PANI/GR nanocomposites with improved electrochemical performance as supercapacitor electrodes [29], facile method to construct a H_2 gas sensor [30], and biosensor for pharmaceutical applications [24]. Though, PANI is a promising conducting polymer, its processability is limited due to the rigid structure which hinders its application. Therefore, it is important to increase the processability of PANI by using substituent groups in the monomer or in the polymer backbone. It is reported that, ortho-substituted groups (—CH_3, —OCH_3, —OC_2H_5) with aniline monomer results in lower conductivity but proceeds enhanced processability due to increased solubility in organic solvents [31].

Poly(o-anisidine) (POA) is a substituted derivative of PANI with methoxy (—OCH_3) group substituted at ortho-position [32]. Due to the electron donor methoxy (—OCH_3) substituent in a benzene ring at ortho position to the amino group this polymer (unlike PANI) is soluble in acids and organic solvents [33]. POA is a relatively new electrically conducting polymer that is generating much interest due to its properties of air stability, electrical conductivity and solubility in organic solvents such as chloroform, acetonitrile, dimethyl formamide and others [34]. Also, the electron donating methoxy functional group in POA with highly conducting graphene filler forms nanocomposite that enhances the charge transport, which finds many promising applications in the field of sensors, supercapacitors, etc. POA has not yet been much explored for the fabrication of biosensors. However, limited attempts have been made to prepare composite films of anisidine with nafion, carbon nanotubes and TiO_2 to explore their use as corrosion resistant coatings [35–38]; potentiometric sensor for K^+ ion [39]. Poly(o-anisidine)-anion composite films have also been prepared as sensing platform for biological molecules [31]. It has been shown for the first time in this work that poly(o-anisidine)/graphene (POA/GR) nanocomposites are suitable for biosensor applications. This simple method of synthesizing nanocomposites improves the chemico-physical properties of the conducting polymer [40]. POA/GR nanocomposites were synthesized with different w/w ratios. The performances of these nanocomposites in electrochemical detection of NADH were tested by cyclic voltammetry (CV). For a comparative study, the POA and GR has also been synthesized, characterised and tested as biosensor electrode material. The nanocomposites showed higher sensing activity when compared to bare polymer and graphene. The study shows that POA/GR nanocomposites exhibited excellent electrocatalytic activity for the oxidation of NADH at low potential range of + 0.045 V in a neutral environment. The improved performance of the nanocomposites is a result of synergy arising from the interaction of the POA and GR sheets. Nanocomposite with POA/GR 3:1 ratio have shown better performance in terms of sensing NADH in comparison to other nanocomposites, which confirms the suitability of POA as a sensing platform for biomolecules.

2. Experimental

2.1. Synthesis of materials

All the chemicals used were of AR grade. Graphene oxide (GO) was synthesized through graphite oxidation with sulphuric acid and potassium permanganate. Reduction of GO to graphene was achieved via refluxing GO with hydrazine sulphate. POA/GR nanocomposites were chemically synthesized by oxidative polymerization of o-anisidine using $(NH_4)_2S_2O_8$ (APS) as oxidant. The o-anisidine to graphene ratio was kept as 1:1, 2:1 and 3:1 w/w ratios, and added in 150 ml of 0.1 M β-naphthalene sulfonic acid (β-NSA) solution, where the solution was cooled to 4 °C in an ice bath. The solution of APS in 50 ml of 0.1 M β-NSA solution was added drop by drop to the above solution. The oxidant to monomer ratio was kept as 1:2 in all the cases. The reaction was continued for 12 h and the dark green precipitate of the nanocomposites recovered from the reaction vessel was filtered and washed using deionized water, methanol and acetone for the elimination of organic impurities. For synthesis of a bare polymer, the same procedure was used without the addition of graphene and the solution was maintained at pH 3. The obtained nanocomposites were assigned as POA/GR11, POA/GR21, and POA/GR31.

2.2. Instrumentation

The X-ray diffraction was carried out using a Rich Siefert 3000 diffractometer with Cu-$K_{\alpha 1}$, radiation ($\lambda = 1.5406$ Å). The morphology and size of the samples were analysed by FESEM and HRTEM using HITACHI SU6600 field emission-scanning electron microscopy and PHILIPS CM200 transmission electron microscopy, respectively. Infrared spectroscopy in the range of 500–4000 cm^{-1} was measured by using a Perkin-Elmer FTIR spectroscopy. UV–visible absorption spectrum of the samples was recorded in the range of 200–1100 nm using a Perkin-Elmer UV–Visible spectroscopy. Raman spectroscopy in the range of 500–3500 cm^{-1} was measured using a Perkin-Elmer Raman spectroscopy. AC impedance measurements were carried out in the frequency range of 20 Hz–1 MHz using Solatron-1260 Impedance Analyzer. The electrochemical experiments were performed on a CHI 1103A electrochemical instrument. Bare glassy carbon electrode (GCE) was used as a working electrode, a platinum wire was used as a counter electrode, and saturated calomel electrode (SCE) was the reference electrode. The samples were first dispersed in acetone by sonication. 1 μl of the dispersion was dropped onto a highly polished GCE and then dried at room temperature.

3. Results and discussion

3.1. Structural and morphological characterisation

XRD patterns of GR, POA, POA/GR11, POA/GR21 and POA/GR31 are presented in Fig. 1(a)–(e). The XRD pattern of graphene shows a peak at 2θ ~ 25.4° (d spacing: 3.534 Å). The broadening of the peak is due to poor ordering of the sheets along the stacking direction which implies that the samples are mainly composed of a few layers of graphene sheets [26]. Fig. 1(b) and (e) shows the XRD patterns of POA and nanocomposites POA/GR11, POA/GR21 and POA/GR31. The XRD pattern of

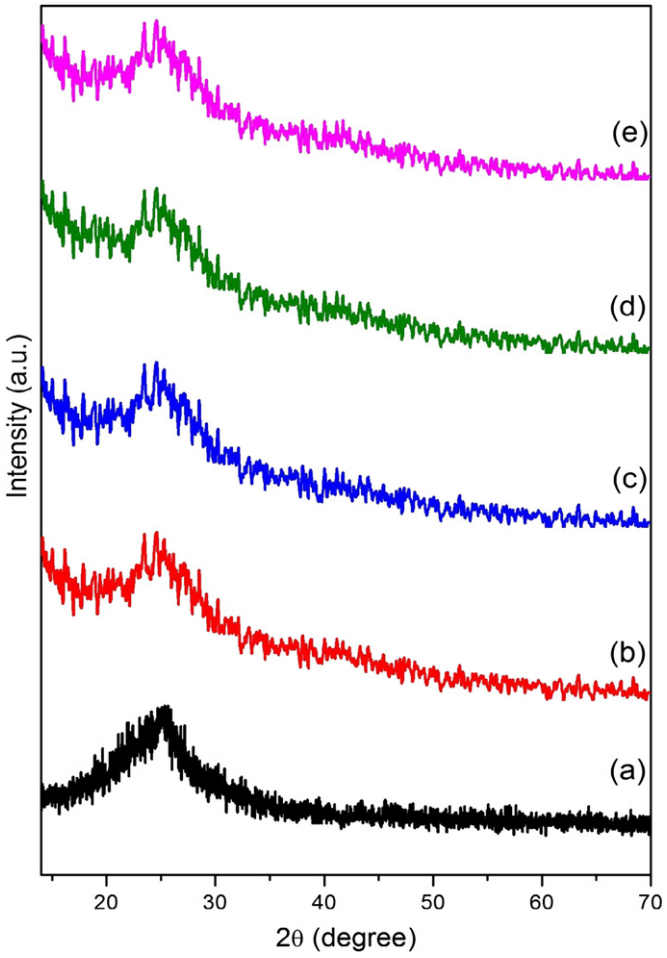

Fig. 1. X-ray diffraction patterns of (a) GR, (b) POA, (c) POA/GR11, (d) POA/GR21 and (e) POA/GR31.

POA shows a medium broad peak centred at 2θ ~ 25.3°, which is a characteristic of the diffraction by an amorphous polymer [41,42]. In XRD patterns of nanocomposites, the observed broadening of the peak centred at 2θ ~ 25° is due to the overlap of polymer diffraction with graphene sheets.

The morphology of the as-synthesized materials was investigated by FESEM and HRTEM technique. Fig. 2(a) shows the FESEM image of the as-prepared graphene sheets with soft wrinkles on the surface. FESEM image of as-synthesized POA reveals the formation of polymer nanofibers in Fig. 2(b). Fig. 2(c) and (d) shows the FESEM images of composites POA/GR11 and POA/GR21 which reveal the growth of POA nanofibers on the surface of graphene sheets. The FESEM image of POA/GR31 shows the porous structure of graphene on which the POA nanofibers are grown. HRTEM was used for more clear identification of morphology of the as-synthesized materials. Fig. 2(e) shows the HRTEM image of graphene where the wrinkled sheets are quite evident. The HRTEM images reveal the interesting morphology of the as-synthesized materials. It can be observed from the HRTEM images of POA and its composites that uniform growth of polymer beads have been linked up and results in the formation of POA nanofibers. Further, HRTEM images of all the composites expose the growth of POA nanofibers on the surface of the graphene sheets. The polymer beads are more clearly visible in HRTEM and their average size is 69 nm. From FESEM images of both as-synthesized POA and POA/GR nanocomposites, the length and diameter of POA nanofibers are comparable and found to be in the range of 1–2 μm and 70 nm, respectively. These nanometre sized particles are suitable to provide relatively short path lengths for charge transport to improve the utilisation of electrodes with high sensing activity. It can be observed that, there is an interesting morphology of the composites, which makes the material a promising candidate for technological applications. The schematic representation of growth of POA nanofibers on the surface of graphene sheets is shown in Scheme 1.

In analysing the morphology of the POA/GR nanocomposites, it is important to take into consideration the electron transport properties of both graphene and o-anisidine monomer in order to determine the molecular binding mechanism. Graphene is a good electron acceptor analogous to other forms of carbon such as, zero-dimensional fullerene (C_{60}) or one-dimensional, single-walled carbon nanotubes. Aniline and its derivatives on the other hand are very good electron donors. It was reported earlier that CNT's can form donor–acceptor complexes in the liquid state when dissolved in tertiary amines and substituted anilines to form stable CNT–aniline complexes [43]. In a similar mechanism for the formation of nanofibers on the graphene nanosheets, the o-anisidine monomer is first adsorbed onto the surfaces of graphene nanosheets due to electrostatic attractions. Oxidation of o-anisidine by APS in the presence of β-NSA as a dopant results in a product with the nanostructures as shown in Fig. 2. It was reported earlier that, aniline dimer, N-phenyl-1,4-phenylenediamine has accelerated the polymerization of the aniline monomer and results in a uniform polymer chain with nanofibrillar morphology on the surface of the graphene [30]. In our work, it can be seen that the POA nanofibers on the surface of graphene sheets are obtained without using any dimer. It may be due to the use of dopant β-NSA which has accelerated the polymerization of monomer and results in nanofibrillar morphology on the surface of graphene sheets [44]. Hence, the graphene nanosheets can be considered as suitable support material for the growth of POA nanofibers by providing a large number of active nucleation sites [45].

3.2. FTIR spectroscopy

The chemical constituents of as-synthesized samples were investigated by FTIR spectroscopy. The FTIR spectra were obtained in the range of 500–4000 cm^{-1} at room temperature. Fig. 3(a)–(e) shows the FTIR spectra of GR, POA, POA/GR11, POA/GR21 and POA/GR31. Fig. 3(a) shows the broad band corresponding to hydroxyl groups (—OH stretching) at 3407 cm^{-1}. The small doublet peaks at 2842 and 2917 cm^{-1} in the FTIR spectra of graphene sheets correspond to symmetric and anti-symmetric —CH_2— vibrations. The small peaks at 1713 cm^{-1}, 1385 cm^{-1} and 1116 cm^{-1} can be attributed to C═O, C—O and —OH of residual —COOH groups of GR sheets [46]. Fig. 3(b) shows the FTIR spectrum of POA with the characteristic band at 3377 cm^{-1} attributed to the O—H stretching vibration. The band at 2929 cm^{-1} can be assigned to the N—H stretching mode. The bands at 1596 and 1506 cm^{-1} were attributed to C═N, C═C stretching in the quinonimine units. The presence of band at 1596 cm^{-1} shows that the polymer is composed of amine unit. The band at 1224 to 1303 cm^{-1} can be assigned to S═O stretching vibration. The band at 1133 cm^{-1} corresponds to stretching vibration of quinoid. The band at 1021 cm^{-1} is due to SO_3^- group of the β-NSA indicating the efficient doping of POA. The bands at 825 cm^{-1} can be attributed to 1,2,4-substitution in the benzenoid rings [42,47,48]. The band at 761 cm^{-1} is assigned to out-of-plane C—H bending vibration [49]. The band at 569 cm^{-1} corresponds to C—H bending in methoxy group. The presence of vibration band of the dopant ion and other characteristic bands confirm that the polymer is in conducting emeraldine salt (ES) phase.

Fig. 3(c)–(e) shows the FTIR spectra of the nanocomposites POA/GR11, POA/GR21, POA/GR31. Few bands of POA and GR have obvious changes due to their interactions. For example, the band at 3407 cm^{-1} in graphene attributing to O—H stretching mode and the band at 3401 cm^{-1} in POA attributing to N—H stretching mode has been shifted

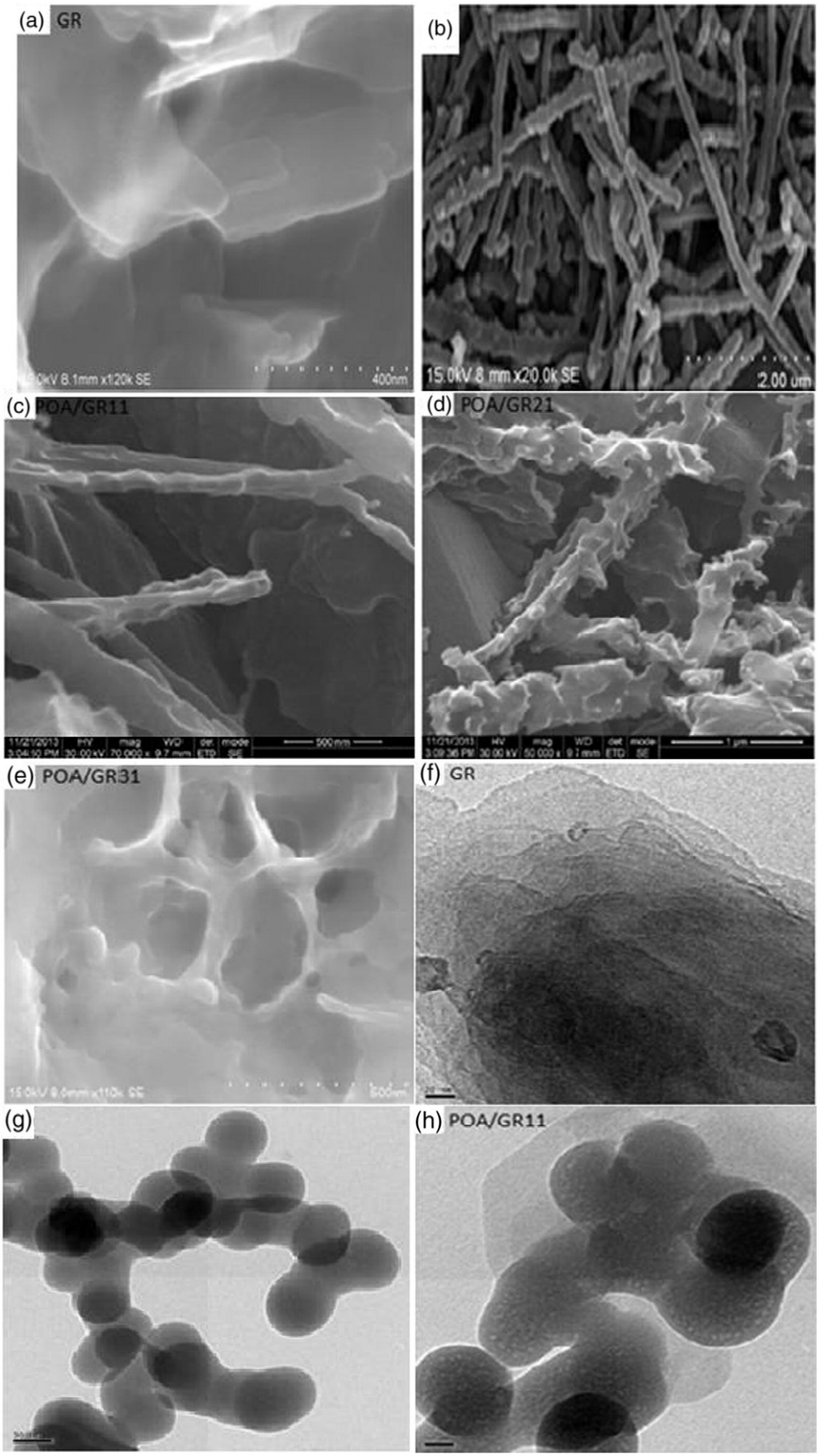

Fig. 2. Field emission scanning electron micrographs (a) GR, (b) POA, (c) POA/GR11, (d) POA/GR21, and (e) POA/GR31; high resolution transmission electron micrographs of (f) GR, (g) POA, (h) POA/GR11, (i) POA/GR21, and (j) and (k) POA/GR31.

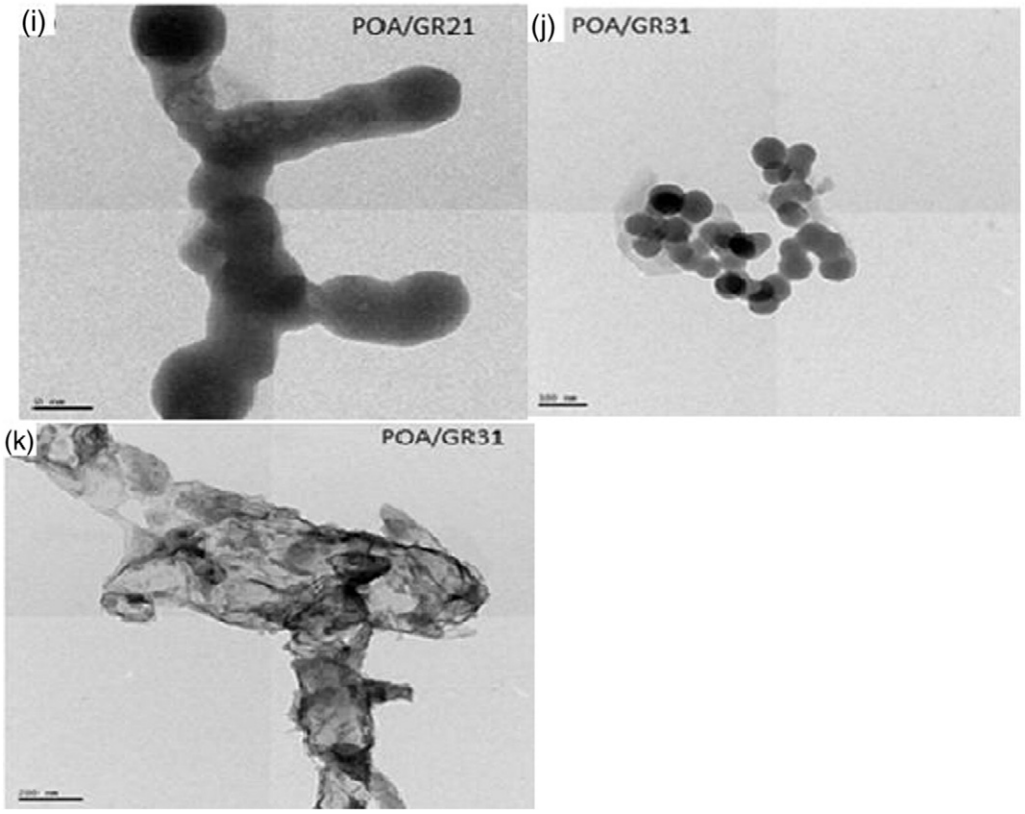

Fig. 2 (*continued*).

to high wave number in the composites. The peak around 1719 cm^{-1} attributed to the C═O in COOH of GR disappeared at the composites. By comparison, it is clear that the spectrum of nanocomposites present the characteristic absorption of both POA and graphene, suggesting that POA was successfully deposited on the surface of graphene sheets and all the nanocomposites are in conducting emeraldine salt (ES) phase.

3.3. Raman spectroscopy

The Raman spectra of GR, POA, POA/GR11, POA/GR21, POA/GR31 are shown in Fig. 4(a)–(e). Raman spectroscopy is considered as a reliable and quick method to characterise graphene. The spectrum of graphene represents the D band, G band and 2D band at 1310 cm^{-1}, 1599 cm^{-1} and 2703 cm^{-1}, respectively. The spectrum of POA presents the following bands corresponding to emeraldine salt phase of the polymer. The two characteristic bands at 1601 and 1598 cm^{-1} are assigned to C—C of the benzene rings and C═C of the quinoid rings. The band at 1513 cm^{-1} is attributed to C═NH^+ of the quinoid protonated di-imine units. The presence of bands at 1373 and 1327 cm^{-1} are attributed to the C—N^+ stretching mode of the polaron radical cation. The band at 1272 cm^{-1} is assigned to C—N of benzenoid and quinoid rings and the band at 1206 cm^{-1} can be attributed to C—H bending of benzenoid rings. All the nanocomposites spectra show the bands attributed to POA and graphene, confirming the occurrence of both these components in the nanocomposites [50,51,48]. Some modifications of the bands of graphene can be clearly observed in response to the presence of POA in the composites. In fact, the D band at 1310 cm^{-1} and G band at 1599 cm^{-1} of graphene is strongly modified by the presence of POA which indicates the interaction between polymer and graphene. Raman spectra confirm the formation of ES phase in all the synthesized materials.

In earlier studies it was demonstrated that the number of graphene layers can be determined by examining the two dimensional (2D) band of the Raman spectrum [46]. In Fig. 4(a), the 2D band at 2703 cm^{-1}, indicates that graphene in our system consists of about five layers [52]. However, because of the high overall coverage of POA nanofibers, the number of graphene layers cannot be accurately determined for POA/GR nanocomposites. Moreover, due to the fact that the Raman spectrum of POA itself exhibits an elevated intensity in the same wavenumber range of the 2D band due to its aromatic structure, further distorts the number of layers measured using Raman spectroscopy. It can be seen that the intensity of 2D band of the nanocomposites increase as the ratio of polymer increases in the composite which further confirms the occurrence of the both POA and GR in the composites.

3.4. UV–Vis spectroscopy

Fig. 5(a)–(e) shows the UV–Vis spectra of the synthesized materials GR, POA, POA/GR11, POA/GR21, POA/GR31. The UV–vis spectrum of POA shows a strong absorption band at 284 nm and a shoulder band around 314 nm. These bands are assigned to the π–π* transition centred on the benzenoid rings (interband transition) [53]. The observed peak at 613 nm is because of n–π* transition from the non-bonding nitrogen lone pair to the conduction band (π*). The peak appearing at 865 nm corresponds to the formation of emeraldine salt phase of the polymer. The UV–vis spectrum of graphene shows a characteristic absorption band at 268 nm corresponding to the π–π* transition. The absorption bands of POA were found to be slightly blue shifted in the spectra of

nanocomposites which manifest the interaction of the polymer structure with graphene.

3.5. Impedance spectroscopy

The room temperature solid state electrical conductivity measurements were taken for POA and its composites. Fig. 6(a)–(d) shows the complex impedance plots between real ($|Z'|$) and imaginary ($|Z''|$) parts of impedance for POA and the nanocomposites POA/GR11, POA/GR21 and POA/GR31. The impedance plot for POA consists of two arcs, a small one at high frequency followed by a large one at low frequency. The arc at higher frequency is due to the conductivity relaxation of the phase with reduced units and at lower frequency is due to the relaxation of the phase with oxidized units. In addition, it was also mentioned that resistivity of the reduced units is lower than that of the oxidized units. The two arcs intersect to give the resistance corresponding to the ac value [54]. The first semicircle, having a smaller resistance, intersects $|Z'|$ axis on the left-hand side and its extension on the right-hand side intersects the same axis at a point termed as R_r (resistance of the phase of reduced units). The extension of the second semicircle, having a higher resistance on the right-hand side intersects the real part of the impedance axis at a point defined as R_o (resistance of the phase of oxidized units). The impedance plots provide clear resolution for the two arcs. It can be seen that for POA/GR composites the diameter of the semicircle reduces remarkably in comparison to bare POA. As the percentage of polymer increases in the composite, the diameter of the semicircle also increases which represents increasing value of resistance.

The proposed equivalent circuit model has been employed by using ZSimpWin software (version 3.21) [55] for fitting of the impedance plane plots for bare POA, POA/GR11, POA/GR21 and POA/GR31 as shown in the inset of Fig. 6. The first small and second large semicircles representing the phases of reduced units and oxidized units have been modelled with equivalent circuit configurations (R_r, CPE_r) and (R_o, CPE_o), respectively. The values of the simulated electrical circuits derived from impedance plane plots of POA and its composites are listed in Table 1. These results indicate that there is a sharp increase in the capacitance and a significant decrease in the resistance of both phases of the composites when compared to bare POA.

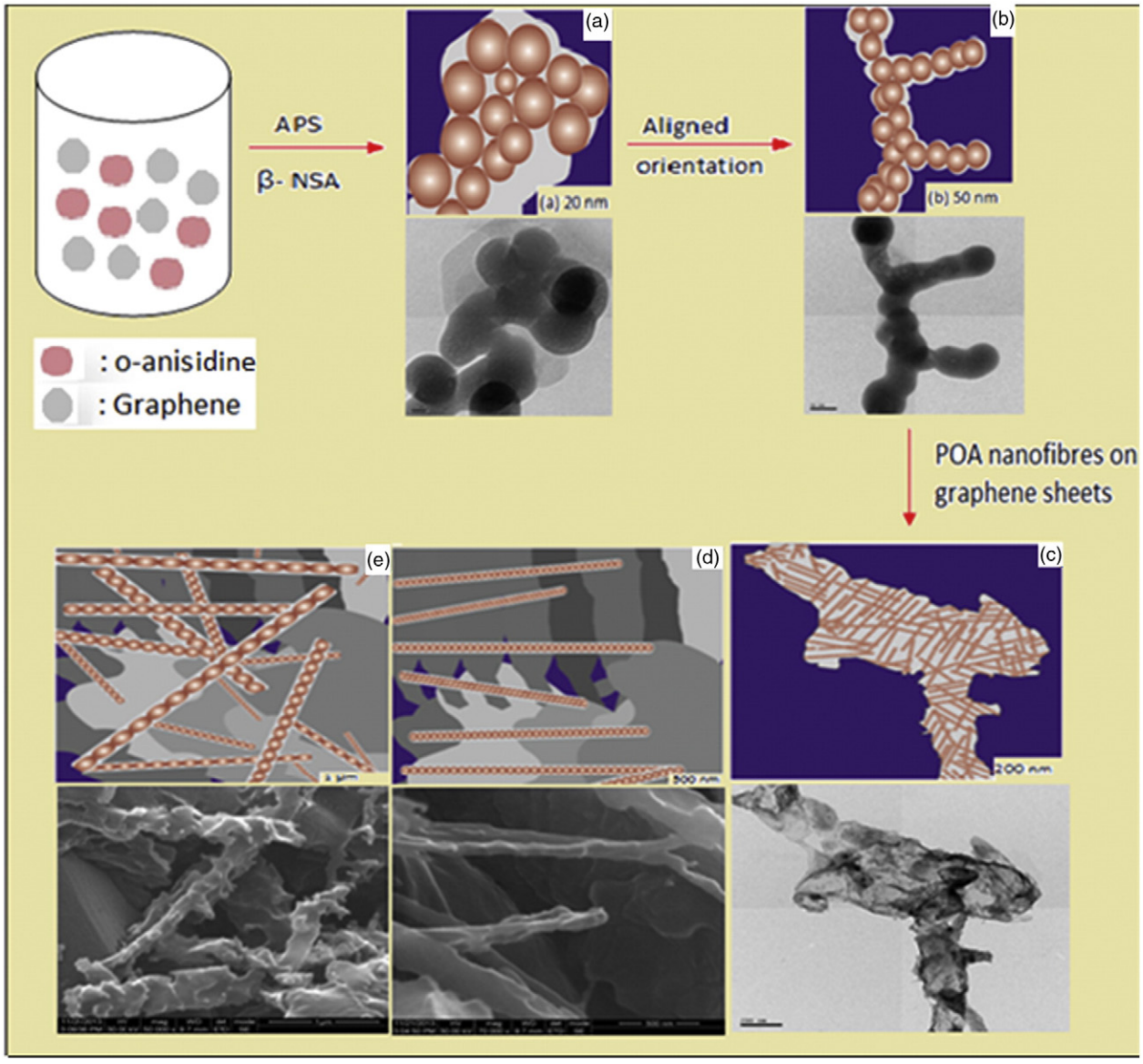

Scheme 1. Schematic diagram illustrating the growth of POA nanofibers on the surface of graphene sheets. (Note: In (d) and (e) different colours of graphene sheets are mentioned for the better visual of stacking of sheets).

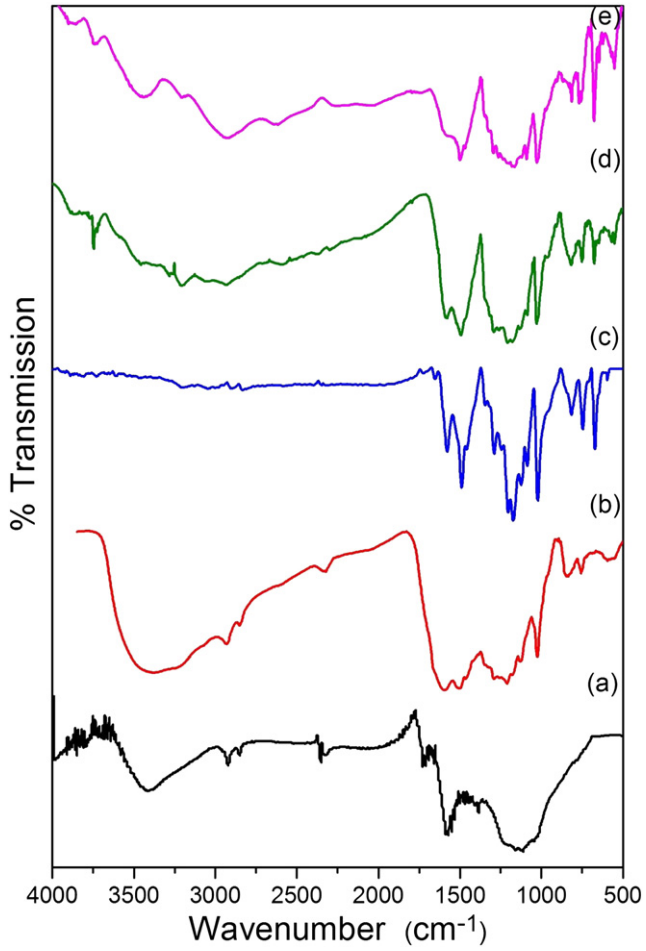

Fig. 3. FTIR spectra of (a) GR, (b) POA, (c) POA/GR11, (d) POA/GR21 and (e) POA/GR31.

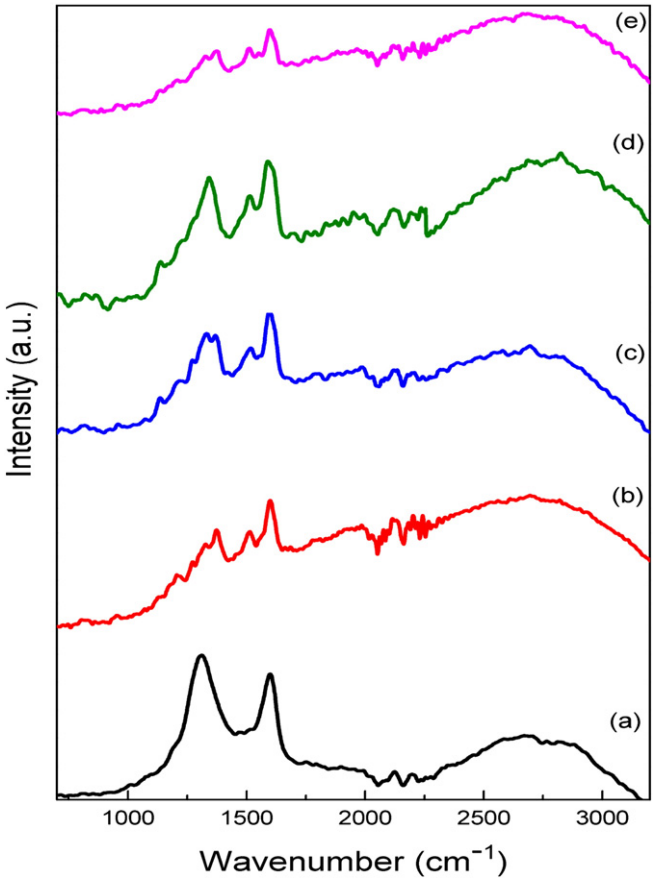

Fig. 4. Raman spectra of (a) GR, (b) POA, (c) POA/GR11, (d) POA/GR21 and (e) POA/GR31.

In conducting polymers there is a strong charge trapping which serves as an electric dipole under the application of an external electric field [56,57]. In presence of this electric field the localised charge carriers can hop to neighbouring sites, which form a continuous network allowing the charges to travel through the entire polymer matrix which enhances electrical conduction [58]. The graphene nanosheets reduce the charge trapping centres, thereby leading to a large number of charge participations which increases the conductivity of the composite. Further, as the percentage of polymer increases in the composite, there is an increase in the resistance of both phases which is due to the overall coverage of POA nanofibers on the surface of graphene sheets.

3.6. Electrochemical biosensing of NADH

3.6.1. Electrocatalytic property

The electrocatalytic response to the oxidation of NADH was detected via cyclic voltammogram (CV). Based on their good biocompatibility, high conductivity and excellent electrochemical behaviour, POA and its nanocomposites were immobilised onto the surface of GCE to be developed as a sensor and applied for the detection of NADH. In order to study the effect of pH on NADH sensor response, solutions of 1 mM NADH with different pH varying from 5.0 to 9.0, were analysed by CV for POA/GR11-modified GCE and the results are shown in Fig. S1[†]. It has been observed that, oxidation of NADH at very low potential with increased peak current was observed at pH 7.0. Based on these observations, phosphate buffer solution (pH 7.0) was chosen as the optimum supporting electrolyte and used in further studies.

Fig. 7 depicts the cyclic voltammograms (CV) for 1.0 mM NADH in 0.1 M PBS (pH 7.0), recorded at 50 mV/s, of (a) GR-modified GCE, (b) POA-modified GCE, (c) POA/GR11-modified GCE, (d) POA/GR21-modified GCE, (e) POA/GR31-modified GCE. The NADH voltammogram obtained for GR-modified GCE (Fig. 7a) and POA-modified GCE (Fig. 7b) showed an oxidation peak with a potential range at about 0.47 and 0.5 V respectively, as previously reported result [39,59]. The observed potentials at POA-modified GCE and GR-modified GCE are still relatively high. The electrocatalytic response of the nanocomposites POA/GR11, POA/GR21 and POA/GR31-modified GCE's are displayed in Fig. 7(c), (d) and

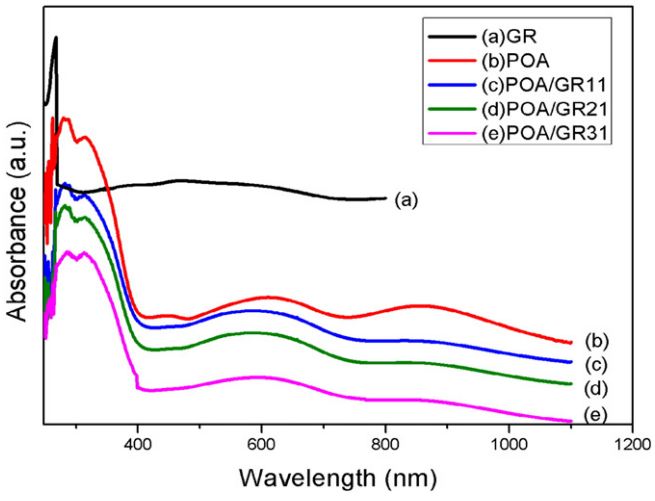

Fig. 5. UV–Vis spectra of (a) GR, (b) POA, (c) POA/GR11, (d) POA/GR21 and (e) POA/GR31.

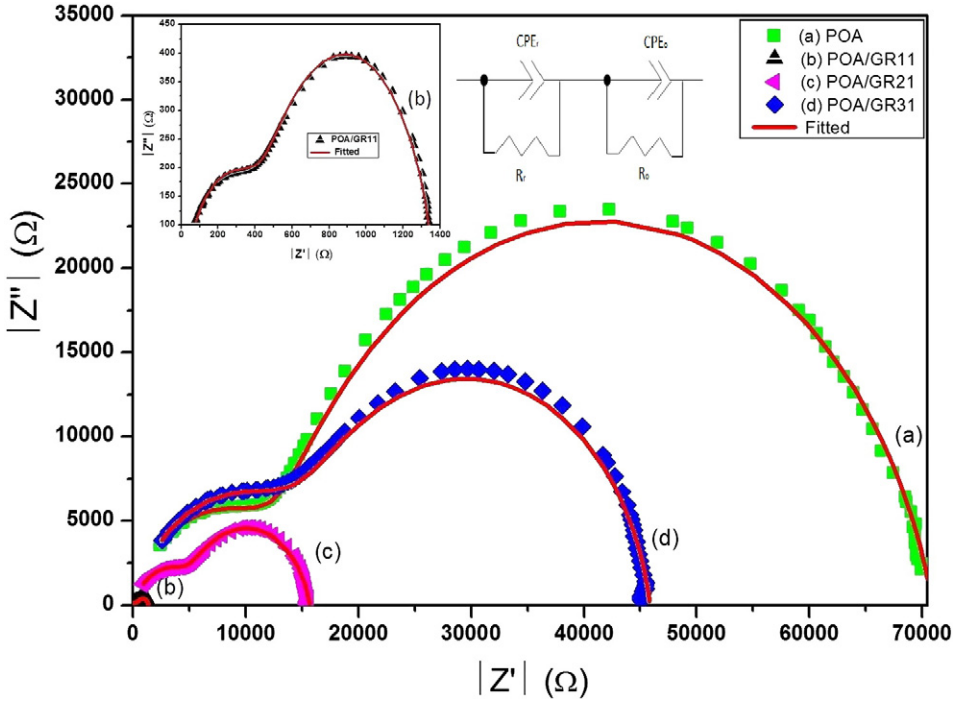

Fig. 6. Complex impedance plots of (a) POA, (b) POA/GR11, (c) POA/GR21 and (d) POA/GR31.

(e). It can be seen that POA/GR-modified GCE's exhibited the lowest oxidation peak potential at about +0.045 V. Comparing with POA-modified GCE and GR-modified GCE the peak current at the POA/GR-modified GCE's were further increased. The oxidation current for POA/GR-modified GCE's are increased in the order of POA/GR11, POA/GR21 and POA/GR31. The increase of the oxidation current to 65 μA in the presence of POA/GR31-modified GCE suggests a faster oxidation process at the electrode surface. Effect of scan rate and the plot of peak current vs. scan rate are shown in Fig. S2(a) and S2(b)†.

The oxidation of NADH proceeds via hydrogen atom transfer followed by electron transfer. An efficient mediator for NADH oxidation should have the structure, which favours hydrogen transfer from NADH to the oxidized form of the mediator. The conducting emeraldine form of POA contains *para*-quinonimine groups, which fulfil the structural requirements for NADH oxidation [31] as shown in Scheme 2. It is well known that NADH is unstable in acidic solution and undergoes hydrolysis to give an enzymatically inactive product at pH < 7.0. In order to develop useful working electrodes for NADH oxidation, it is essential to maintain pH 7.0, whereas, the emeraldine form of POA is usually deprotonated and nonconducting at pH > 4. Therefore, it is necessary to synthesis composites of POA with carbon based materials such as CNT, graphene, etc., in order to maintain the electrocatalytic activity of the polymer at pH 7.0, which can enhance the efficiency of polymer based biosensors by effectively interacting with the analytes (biomolecules) present in the reaction. It can be seen that, compared to POA prepared without graphene, the POA/GR nanocomposites showed significantly improved electrochemical behaviour at neutral pH 7.0 for the detection of NADH. The faster oxidation process could be attributed to the electrostatic attraction between the positively charged polymer and negatively charged NADH molecules [60]. On the other hand, graphene with a large surface-to-volume ratio and high efficiency of electronic and ionic transfer enhanced the conduction pathways and allowed efficient electron transport, which facilitated the charge transfer between NADH and the electrode surface [61]. In NADH biosensor on the basis of POA/GR nanocomposites, the growth of polymer nanofibers on the surface of graphene nanosheets allow the formation of three-dimensional electronic conductive network by the close contact between polymer and graphene which enhanced the charge transfer capacity and lead to the increase of oxidation of NADH on the electrode surface. Higher oxidation current was observed in the case of POA/GR31-modified GCE due to the reason that in the ratio of 3:1, POA could allow the large number of hydrogen transfer from NADH, and graphene nanosheets enhances the charge transfer process which suggests the suitability of polymer and it's composite to be a good biosensor material. Lower potential range compared to literature reports indicates the facile kinetics of oxidation at the POA/GR-modified electrodes. It has been well established that NADH undergoes a two-electron (2e) and one proton oxidation in aqueous solution to yield the corresponding nicotinamide (NAD^+) [62]. Scheme 2 represents the mediated electron transfer on a POA/GR-modified electrode during the oxidation of NADH. The simplified oxidation mechanism could be expressed by Eq. (1)

$$NADH - 2e^- - H^+ \rightarrow NAD^+. \quad (1)$$

Table 1
Fitting parameters calculated from the equivalent circuit model.

	POA	POA/GR11	POA/GR21	POA/GR31
CPE_r (F)	7.695×10^{-10}	1.174×10^{-7}	3.232×10^{-9}	1.01×10^{-9}
R_r (Ω)	11,232.760	395.520	4226.911	9080.690
CPE_o (F)	5.982×10^{-10}	1.458×10^{-7}	3.652×10^{-8}	1.01×10^{-9}
R_o (Ω)	69,910.780	1357.080	15,458.420	31,332.050

3.6.2. Differential pulse voltammetry response of NADH at POA/GR31-modified GCE

To investigate the dependence between peak currents and NADH concentrations, differential pulse voltammetry (DPV) was chosen as more sensitive voltammetric technique in comparison with cyclic voltammetry. This procedure involves an optimisation of the experimental parameters which affects the peak current such as modulation amplitude, modulation time and scan rate. During optimisation, each parameter was changed while the others were kept constant. Peak current was

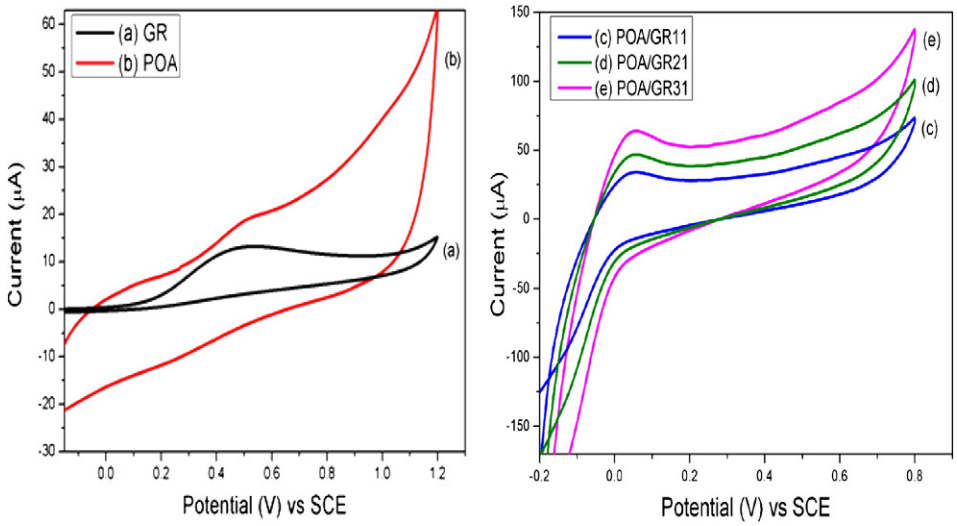

Fig. 7. Cyclic voltammograms of different materials modified electrodes in 0.1 M PBS (pH 7.0) containing 1 mM NADH at the scan rate of 50 mV/s. (a) GR, (b) POA, (c) POA/GR11, (d) POA/GR21 (e) POA/GR31.

found to be increased with the increasing of modulation amplitude accompanied by the widening of peak width at the same time. When the modulation amplitude is higher than 0.05 V, the peak becomes much wider. As for the modulation time, peak currents decreased with an increasing of modulation time and the most stable peak current was observed at about 0.02 s. Table 2 shows the studied range of DPV parameters and their optimum values which were used for DPV calibration.

Applying the optimised experimental conditions as discussed above, DPV of the POA/GR31-modified GCE in PBS (pH 7.0) with different concentrations of NADH is shown in Fig. 8. It could be observed that with the addition of NADH, a peak at around +0.045 V emerged. It clearly revealed that, the current has increased and the peak potential was not shifted with increasing NADH concentration. The calibration curve obtained for NADH concentration vs. peak current is shown in the inset of Fig. 8 was linear in the concentration range of 0.166 to 1.772 μM. The results showed that the POA/GR31-based sensor displays a correlation coefficient of 0.9932 with a sensitivity of 47.1 μA μM^{-1} which could be considered as quite high when compared with the literature. A low detection limit (LOD) of 1.3 μM and the limit of quantification (LOQ) of 4.97 μM were obtained with a signal to noise ratio of 3 which was comparable to the reported literature [63–66]. The high performance in the detection of NADH indicates that the POA/GR nanocomposites greatly enhance the electron transfer between NADH and

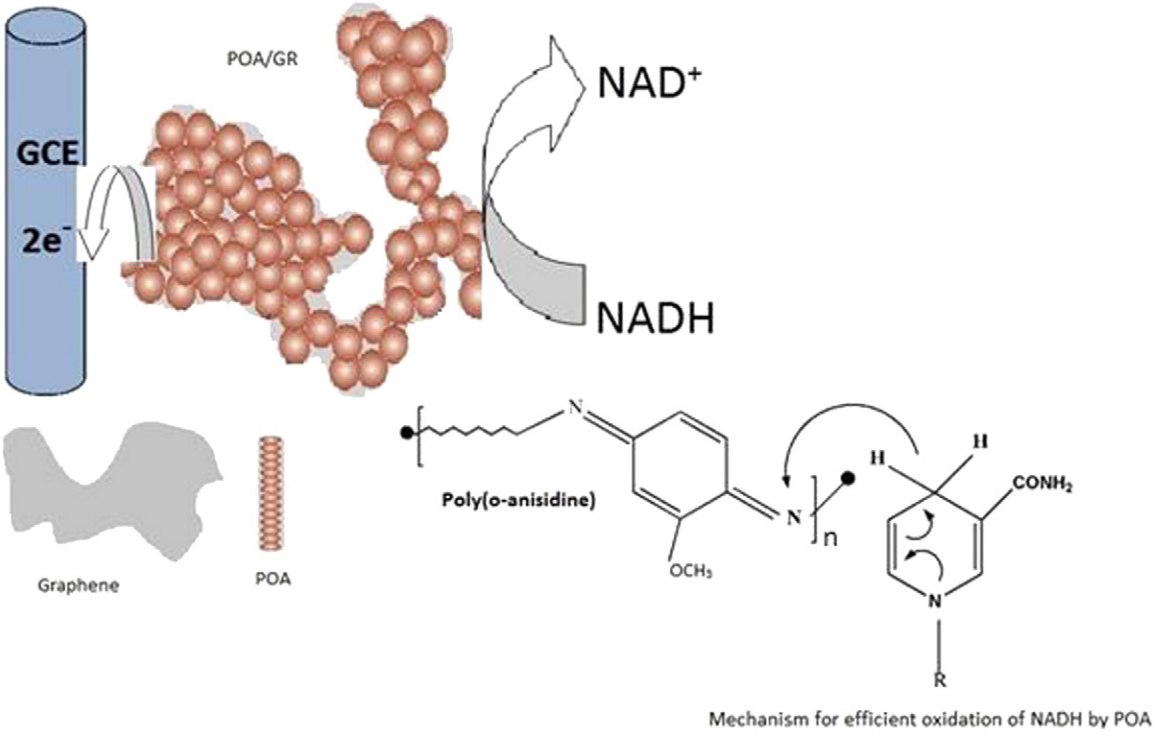

Scheme 2. Mediated electron transfer on a POA/GR-modified electrode during NADH oxidation.

Table 2
Experimental parameters examined in the optimization of the DPV.

Parameters	Range studied	Optimum value
Modulation amplitude (V)	0.02–0.10	0.05
Modulation time (s)	0.01–0.05	0.02
Scan rate (V s^{-1})	0.01–0.10	0.05

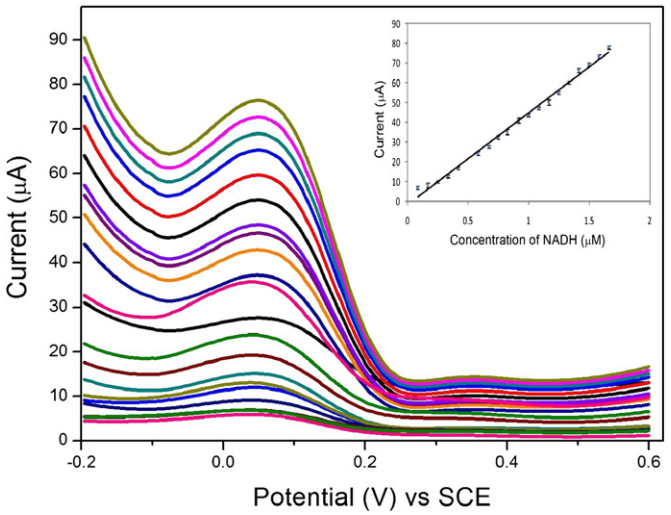

Fig. 8. Differential pulse voltammograms of POA/GR31-modified GCE in 0.1 M PBS (pH 7.0) containing 0.166, 0.249, 0.332, 0.416, 0.499, 0.582, 0.666, 0.749, 0.832, 0.915, 0.999, 1.082, 1.165, 1.248, 1.331, 1.414, 1.497, 1.580, 1.66, 1.772 μM NADH (*from bottom to top*). *Inset: Plot of peak current vs. concentration of NADH* (the error bars are constructed for three measurements).

electrode [67]. Table 3 presents the main performance of published data about NADH sensors based on polymers and composite materials. By comparison, the NADH sensor presented in this work exhibits higher sensitivity with low detection limit.

3.6.3. Amperometric response of NADH at POA/GR modified GCE

On the basis of the voltammetric results described above, it is likely that chronoamperometric detection of NADH by POA/GR-modified GCE is possible. According to the potential dependence of the NADH determined by electrocatalytic oxidation current at stirring conditions, the optimum electrode potential was selected as +0.045 V versus SCE for chronoamperometric measurements in order to obtain the stability. Fig. 9 displays the chronoamperometric response of the POA/GR-modified GCE's upon the addition of different concentrations of NADH. A successive addition of NADH to continuously stirred 0.1 M PBS (pH 7.0) produces a significant increase in the current with increase in the concentration of NADH (0.166 to 1.772 μM). The oxidation current for the composite modified GCE's are increased in the order of POA/GR11, POA/GR21 and POA/GR31. The peak current gradually increased and was proportional to the NADH concentrations as shown in the inset of Fig. 9. The results showed that the POA/GR31-based sensor displays a correlation coefficient of 0.9967. It is also observed that amperometric response was stable for about 10 min. This is a proof that no passivation of the electrode surface occurred. This phenomenon could be attributed to the presence of composite, which does not favour the accumulation of the oxidation product, NAD^+ on the electrode surface [59]. The good stability of the sensor seems to be an intriguing feature when compared to other NADH sensors.

3.6.4. Reproducibility and stability of POA/GR-modified GCE

The reproducibility and stability of the sensor were also investigated by the amperometric method. The reproducibility of the POA/GR31-modified GCE was evaluated from the current response at +0.045 V vs. SCE and the relative standard deviation (RSD) value of 3.53% was observed when the experiments have been repeated for 10 times for concordant values of 1 mM NADH. The fabrication reproducibility was also determined with NADH at five different modified electrodes prepared independently and 5.9% of RSD was achieved. The results demonstrate that the reproducibility

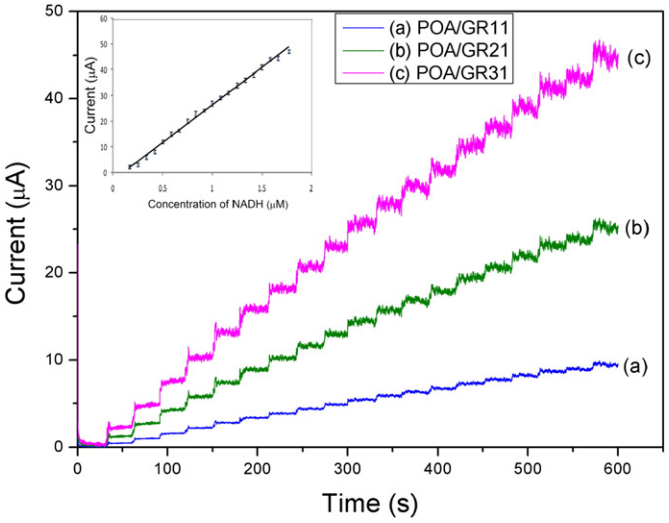

Fig. 9. Chronoamperometric response of (a) POA/GR11, (b) POA/GR21 and (c) POA/GR31-modified GCE's. *Inset: Plot of peak current vs. concentration of NADH* (the error bars are constructed for three measurements).

Table 3
Comparison of the efficiency of some modified electrodes used in electrocatalysis of NADH.

Working electrode	E_p(V)	Sensitivity	Detection limit (μM)	Reference
Poly(1,2diaminobenze)/MWCNT/GCE	+0.070	–	–	[62]
Poly-phenothiazine/GCE	+0.200	1.82 μA mM^{-1}	3.40	[63]
CNT-chitosan/GCE	+0.400	–	3.00	[64]
Nile blue/ordered mesoporous carbon composite/GCE	−0.100	0.648 μA mM^{-1}	1.20	[65]
CNT/GCE	+0.330	–	–	[66]
Highly ordered mesoporous carbon/GCE	+0.250	6.51 nAμM^{-1}	1.61	[67]
Chemically reduced graphene oxide/GCE	+0.450	2.68 μA mM^{-1} cm^{-2}	10.00	[68]
Ionic liquid functionalized graphene/GCE	+0.330	37.43 μA mM^{-1} cm^{-2}	–	[59]
Water treated CNT/Chitosan/GCE	0.000	3.2 mA M^{-1} cm^{-2}	4.00	[69]
Graphene/GCE	+0.500	12.6 μA mM^{-1}	20.00	[70]
Polyaniline/polyvinylsulphonate	+0.100	–	–	[71]
POA/GR/GCE	+0.045	47.1 μA $μM^{-1}$	1.30	Present study

of the sensor was acceptable and had great precision. The long term stability of POA/GR31-modified GCE was studied for the electrodes stored for 15 days under ambient conditions in 0.1 M PBS (pH 7.0). After this time period the sensor retained 92.7% of its initial response, indicating good long-term stability due to strong interaction of POA with graphene nanosheets.

3.6.5. Interference study of POA/GR31-modified GCE

Resistance to interference is important for electrochemical sensors. Interference from electroactive compounds typically present in physiological samples (e.g. ascorbic acid (AA)) commonly hinders the accurate determination of NADH. The selectivity of the biosensor was examined in the presence of AA. The amperometric measurements were determined for both NADH and AA at POA/GR31-modified GCE with a fixed potential of + 0.045 V. Fig. 10 shows the amperometric current response of POA/GR31-modified GCE to successive addition of 1.0 mM NADH and 1 mM AA in 0.1 M of PBS (pH 7.0) at the applied potential of + 0.045 V vs. SCE. The first three steps correspond to the addition of different concentrations of NADH (0.166, 0.249, 0.332 μM); the next two steps were conducted with the addition of AA (5, 10 μM); again two steps were conducted with the addition of NADH (0.499, 0.582 μM); and then two more steps were performed for AA (15, 20 μM) and finally further successive iterations were conducted for the addition of NADH. It could be seen that for each addition of NADH, there is an observable increase in the value of current and no response was obtained for the addition of AA. It showed that catalytic current of NADH oxidation at POA/GR-modified GCE under applied potential of + 0.045 V was achieved and no current response was obtained at this applied potential for AA. Therefore, + 0.045 V was chosen as the optimised applied potential for sensing NADH without interference from AA.

3.6.6. Model sample analysis

In order to estimate the accuracy of the proposed analytical technique, the standard additions method [70] was performed using POA/GR31-modified GCE. Absolute NADH content of 0, 0.2, 0.4, 0.6, 0.8, 1.0 μM spiked with ascorbic acid was analysed and diluted to 20 ml with PBS (pH 7.0). The average results for six replicate measurements with confidence interval for 95% probability, residual errors and uncertainty in the regression analysis are summarized in Table 4. It is concluded that the proposed method is suitable for determination of NADH in the presence of ascorbic acid.

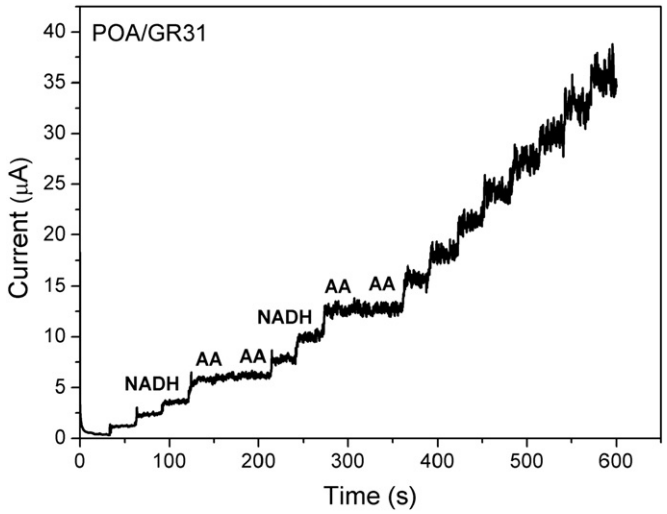

Fig. 10. Chronoamperometric response of POA/GR31-modified GCE with NADH and AA.

4. Conclusion

In this paper, the response of the poly(o-anisidine)/graphene nanocomposites modified GCE for the sensing of NADH has been explored for the first time. The synthesized nanocomposites are characterised by XRD, FESEM, HRTEM, FTIR, Raman and UV–vis spectroscopy. With the use of impedance spectroscopy technique, the resistance of oxidized and reduced units has been deduced and their characteristic properties have been investigated. The composite modified electrodes showed high electrocatalytic activity with low potential range towards the oxidation of NADH in a neutral environment compared with that of the bare POA-modified GCE and GR-modified GCE. Higher catalytic current is observed for nanocomposite POA/GR31-modified GCE confirms the suitability of polymer for electrochemical detection of NADH. POA/GR31-modified GCE exhibited very high sensitivity of 47.1 μA μM^{-1} with low detection limit of 1.3 μM and limit of quantification of 4.97 μM for detection of NADH. Modified electrodes exhibited excellent analytical performance for NADH detection with good stability and reproducibility. The effect of interfering species commonly found in biological samples, such as ascorbic acid did not interfere with the analytical response of the coenzyme. The accuracy of the proposed analytical technique was estimated by standard additions method. POA/GR nanocomposite seem extremely attractive and potent to be used in numerous dehydrogenase-based bioelectrochemical devices and have the potential to be employed in several applications in the field of biosensors, biofuels and bioreactors in the near future.

Table 4
Determination results of NADH spiked in ascorbic acid (n = 6).

Added (μM)	Found* (μM)	Confidence interval for 95% probability** (μM)	Residual error
0.0	0.007	0.007 ± 0.002	0.01
0.2	0.193	0.193 ± 0.011	−0.10
0.4	0.377	0.377 ± 0.012	−0.11
0.6	0.617	0.617 ± 0.013	0.15
0.8	0.829	0.829 ± 0.018	0.17
1.0	0.976	0.976 ± 0.022	−0.20
		Total residual error***	0.11
		Uncertainty in the regression analysis	±0.16

* Average for six replicate measurements (n = 6): $\bar{x}$.
** [72] Calculated according ($x_f \pm t \times SD/\sqrt{n}$); t = 2.0150.
*** [73] Calculated according, $R = \Sigma(\hat{y}_i - y_i)^2$.

Acknowledgements

One of the authors (D.S.) thanks DST (IF 120706), New Delhi for the financial support received in the form of INSPIRE fellowship. The authors thank the support from NCNSNT, University of Madras and SAIF, IIT, Chennai, India.

Appendix A. Supplementary data

†Electronic Supplementary Information (ESI) available: Effect of pH and effect of scan rate. Supplementary data to this article can be found online at doi:.

References

[1] H.R. Zare, N. Nasirizadeh, M. Mazloum-Ardakani, M. Namazian, Electrochemical properties and electrocatalytic activity of hematoxylin modified carbon paste

electrode toward the oxidation of reduced nicotinamide adenine dinucleotide (NADH), Sensors Actuators B 120 (2006) 288–294.
[2] L.M. Smyth, J. Bobalova, M.G. Mendoza, C. Lew, V.N. Mutafova-Yambolieva, Release of beta-nicotinamide adenine dinucleotide upon stimulation of post-ganglionic nerve terminals in blood vessels and urinary bladder, J. Biol. Chem. 279 (2004) 48893–48903.
[3] R.A. Billington, S. Bruzzone, A. De Flora, A.A. Genazzani, F. Koch-Nolte, M. Ziegler, E. Zocchi, Emerging functions of extracellular pyridine nucleotides, Mol. Med. 12 (2006) 324–327.
[4] H.K. Chenault, G.M. Whitesides, Regeneration of nicotinamide cofactors for use in organic synthesis, Appl. Biochem. Biotechnol. 14 (1987) 147–149.
[5] M. Zhang, C. Mullens, W. Gorski, Co-immobilization of dehydrogenase and their co-factors in electrochemical biosensors, Anal. Chem. 79 (2007) 2446–2450.
[6] R. Scipioni, M. Pumera, M. Boero, Y. Miyahara, T. Ohno, Investigation of the mechanism of adsorption of β-nicotinamide adenine dinucleotide on single-walled carbon nanotubes, J. Phys. Chem. Lett. 1 (2009) 122–125.
[7] M. Pumera, R. Scipioni, H. Iwai, T. Ohno, Y. Miyahara, M. Boero, A mechanism of adsorption of β-nicotinamide adenine dinucleotide on graphene sheets, Chem. Eur. J. 15 (2009) 10851–10856.
[8] J. Zhu, X. Chen, W.S. Yang, A high performance electrochemical sensor for NADH based on graphite nanosheets modified electrode, Sensors Actuators B Chem. 150 (2010) 564–568.
[9] Q. Wang, H. Tang, Q.J. Xie, L. Tan, Y.Y. Zhang, B.M. Li, et al., Room temperature ionic liquids / multi-walled carbon nanotubes / chitosan composite electrode for electrochemical analysis of NADH, Electrochim. Acta 52 (2007) 6630–6637.
[10] Y. Fan, X. Yang, C.P. Yang, J.H. Liu, Au–TiO_2/graphene nanocomposite film for electrochemical sensing of hydrogen peroxide and NADH, Electroanalysis 24 (2012) 1334–1339.
[11] L.N. Pelster, M.T. Meredith, S.D. Minteer, Nicotinamide adenine dinucleotide oxidation studies at multiwalled carbon nanotube/polymer composite modified glassy carbon electrodes, Electroanalysis 24 (2012) 1011–1018.
[12] H. Teymourian, A. Salimi, R. Hallaj, Recent advances in dehydrogenase biosensors based on carbon nanotube modified electrodes, Biosens. Bioelectron. 33 (2012) 60–68.
[13] H. Teymourian, A. Salimi, R. Hallaj, Electrocatalytic oxidation of NADH at electrogenerated NAD^+ oxidation product immobilized onto multiwalled carbon nanotubes/ionic liquid nanocomposite: application to ethanol biosensing, Talanta 90 (2012) 91–98.
[14] W. Jia, L. Su, Y. Lei, Pt nanoflower/polyaniline composite nanofibers based urea biosensor, Biosens. Bioelectron. 30 (2011) 158–164.
[15] A.S. Leppanen, C. Xu, J. Liu, X. Wang, M. Pesone, S. Willfor, Anionic polysaccharides as templates for the synthesis of conducting polyaniline and as structural matrix for conducting biocomposites, Macromol. Rapid Commun. 34 (2013) 1056–1061.
[16] R.S. Diggika, M.V. Kulkarni, G.M. Kale, B.B. Kale, Formation of multifunctional nanocomposites with ultrathin layers of polyaniline (PANI) on silver vanadium oxide (SVO) nanospheres by in situ polymerization, J. Mater. Chem. A1 (2013) 3992–4001.
[17] V.K. Shukla, P. Yadav, R.S. Yadav, P. Mishra, A.C. Pandey, A New class of PANI-Ag core–shell nanorods with sensing dimensions, Nanoscale 4 (2012) 3886–3893.
[18] Y. Luo, D. Kong, Y. Jia, J. Luo, Y. Lu, D. Zhang, K. Qiu, C.M. Li, Self-assembled graphene @ PANI nanoworm composites with enhanced supercapacitor performance, RSC Adv. 3 (2013) 5851–5859.
[19] M. Li, X. Huang, C. Wu, H. Xu, P. Jiang, T. Tanaka, Fabrication of two-dimensional hybrid sheets by decorating insulating PANI on reduced graphene oxide for polymer nanocomposites with low dielectric loss ad high dielectric constant, J. Mater. Chem. 22 (2012) 23477–23484.
[20] J.X. Huang, R.B. Kaner, A general chemical route to polyaniline nanofibers, J. Am. Chem. Soc. 126 (2004) 851–855.
[21] W. Yan, X. Feng, X. Chen, X. Li, J. Zhu, A selective dopamine biosensor based on AgCl@ polyaniline core–shell nanocomposites, Bioelectrochemistry 72 (2008) 21–27.
[22] X. Wang, T. Yang, X. Li, K. Jiao, An electrochemical DNA microbiosensor based on succinimide-modified acrylic microspheres, Biosens. Bioelectron. 26 (2011) 2953–2959.
[23] Mohammed Zourob, Sauna Elwary, Anthony Turner, Principles of Bacterial Detection: Biosensors, Recognition Receptors and Microsystems, 2008. 391.
[24] K. Radhapyari, P. Kotoky, M.R. Das, R. Khan, Graphene–polyaniline nanocomposite based biosensor for detection of antimalarial drug artesunate in pharmaceutical formulation and biological fluids, Talanta 111 (2013) 47–53.
[25] S. Stankovich, D.A. Dikin, G.H.B. Dommett, K.M. Kohlhaas, E.J. Zimney, E.A. Stach, Graphene based composite materials, Nature 442 (2006) 282–286.
[26] Jaidev, S. Ramaprabhu, Poly(p-phenylenediamine)/graphene nanocomposites for supercapacitor applications, J. Mater. Chem. 22 (2012) 18775–18783.
[27] H. Kim, A.A. Abdala, C.W. Makosko, Graphene/polymer nanocomposites, Macromolecules 43 (2010) 6515–6530.
[28] J. Yan, T. Wei, B. Shao, Z. Fan, W. Qian, M. Zhang, F. Wei, Preparation of a graphene nanosheet/polyaniline composite with high specific capacitance, Carbon 48 (2010) 487–493.
[29] H. Gómez, M.K. Ram, F. Alvi, P. Villalba, E. Stefanakos, Ashok Kumar, Graphene-conducting polymer nanocomposite as novel electrode for supercapacitor, J. Power Sources 196 (2011) 4102–4108.
[30] Al. Mashat, K. Shin, K. Kalantr-zadeh, J.D. Plessis, S.H. Han, R.W. Kojima, R.B. Kaner, D. Li, X. Gou, S.J. Ippolito, W. Wlodarski, Graphene/polyaniline nanocomposite for hydrogen sensing, J. Phys. Chem. C 114 (2010) 16168–16173.
[31] B. Angaleeswari, R.M. Dura Amirtham, T. Jeevithaa, V. Vaishnavi, T. Eevera, Sheela Berchmans, V. Yegnaraman, Poly(o-anisidine)-anion composite films as sensing platform for biological molecules, Sensors Actuators B Chem. 129 (2008) 558–565.
[32] D. Patila, P. Patila, Y. Seo, Y. Hwang, Poly(o-anisidine)-tin oxide nanocomposite: synthesis, characterization and application to humidity sensing, Sensors Actuators B 148 (2010) 41–48.
[33] J. Jiang, L. Hong Ai, A. Liu, A novel poly(o-anisidine)/$CoFe_2O_4$ multifunctional nanocomposite: preparation, characterization and properties, Synth. Met. 160 (2010) 333–336.
[34] L. Valentini, V. Bavastrello, E. Stura, I. Armentano, C. Nicolini, J.M. Kenny, Sensors for inorganic vapour detection based on carbon nanotubes and poly(o-anisidine) nanocomposite material chemical physics material, Chem. Phys. Lett. 383 (2004) 617–622.
[35] P. Pawar, A.B. Gaikwad, P. Patil, Corrosion protection aspects of electrochemically synthesized poly(o-anisidine-co-o-toluidine) coatings on copper, Electrochim. Acta 52 (2007) 5958–5967.
[36] S. Carrara, V. Bavastrello, D. Ricci, E. Stura, C. Nicolini, Improved nanocomposite materials for biosensor applications investigated by electrochemical impedance spectroscopy, Sensors Actuators B 109 (2005) 221–226.
[37] P. Bertoncello, A. Notargiacomo, D.J. Riley, M.K. Ram, C. Nicolini, Preparation, characterization and electrochemical properties of Nafion doped poly(ortho-anisidine) (POAS) Langmuir–Schaefer films, Electrochem. Commun. 5 (2003) 787–792.
[38] Y. Jafaria, M.S. Nooshabad, S.M. Ghoreishi, Electropolymerized coatings of poly(o-anisidine) and poly(o-anisidine)-TiO_2 nanocomposite on aluminium alloy 3004 by using the galvanostatic method and their corrosion protection performance, Polym. Adv. Technol. 25 (2014) 279–287.
[39] J.E. Zachara, R. Toczyłowska, R. Pokrop, M. Zagrska, A. Dybko, W. Wroblewski, Miniaturised all-solid-state potentiometric ion sensors based on PVC membranes containing conducting polymers, Sensors Actuators B Chem. 101 (2004) 207–212.
[40] V. Bavastrelloa, V. Erokhin, S. Carrara, F. Sbrana, D. Ricci, C. Nicolini, Morphology and conductivity in poly(ortho-anisidine)/carbon nanotubes nanocomposite films, Thin Solid Films 468 (2004) 17–22.
[41] A.A. Khan, S. Shaheen, U. Habiba, Synthesis and characterization of poly-o-anisidine Sn(IV) tungstate: a new and novel 'organic–inorganic' nano-composite material and its electro-analytical applications as Hg(II) ion-selective membrane electrode, J. Adv. Res. 3 (2012) 269–279.
[42] L.H. Mahajan, S.T. Mhaske, Composite microspheres of poly(o-anisidine)/TiO_2, Mater. Lett. 68 (2012) 183–186.
[43] Y. Sun, S.R. Wilson, D.I. Schuster, High dissolution and strong light emission of carbon nanotubes in aromatic amine solvents, J. Am. Chem. Soc. 123 (2001) 5348–5349.
[44] Z. Shahnavaz, F. Lorestani, Y. Alias, Polypyrrole–$ZnFe_2O_4$ magnetic nano-composite with core–shell structure for glucose sensing, Appl. Surf. Sci. 317 (2014) 622–629.
[45] R.J. Seresht, M. Jahanshahi, A. MoradRashidi, A.A. Ghoreyshi, Synthesis and characterization of thermally-reduced graphene, Iran. J. Energy Environ. 4 (1) (2013) 53–59.
[46] K.S. Kim, Y. Zho, H. Jang, S.Y. Lee, J.M. Kim, K.S. Kim, J.H. Ahn, P. Kim, J.Y. Choi, B.H. Hong, Large-scale patter growth of graphene films for stretchable transparent electrodes, Nature 457 (2009) 706–710.
[47] Q. long pham, Y. Haldorai, V.H. Nguyen, D. Tuma, J.J. Shim, Facile synthesis of poly(p-phenylenediamine)/MWCNT nanocomposites and characterization for investigation of structural effects of carbon nanotubes, Bull. Mater. Sci. 34 (2011) 37–43.
[48] G.C. Marjanovic, B. Marjanovic, P. Bober, Z. Rozlivkova, J. Stejskal, M. Trchova, J. Prokes, The oxidative polymerization of *p*-phenylenediamine with silver nitrate: toward highly conducting micro/nanostructured silver/conjugated polymer composites, J. Polym. Sci. A Polym. Chem. 49 (15) (2011) 3387–3403.
[49] T. Sulimenko, J. Stejskal, J. Prokes, Poly(phenylenediamine dispersions), J. Colloid Interface Sci. 236 (2001) 328–334.
[50] R.H. Sestrem, D.C. Ferreira, R. Landers, M.L.A. Temperini, G.M.D. Nascimento, Structure of chemically prepared poly-(*para*-phenylenediamine) investigated by spectroscopic technique, Polymer 50 (2009) 6043–6048.
[51] J.J. Wang, J. Jiang, B. Hu, S.H. Yu, Uniformly shaped poly(*p*-phenylenediamine) microparticles: shape-controlled synthesis and their potential application for the removal of lead ions from water, Adv. Funct. Mater. 18 (2008) 1105–1111.
[52] A. Gupta, G. Chen, P. Joshi, S. Tadigadapa, P.C. Eklund, Raman scattering from highly-frequency phonons in supported n-graphene layer films, Nano Lett. 6 (12) (2006) 2667–2673.
[53] M. Nandi, S.K. Das, S. Giri, A. Bhaumik, Fe(III)-containing mesoporous poly-(p-phenylenediamine): synthesis, characterization and magnetic properties, Microporous Mesoporous Mater. 142 (2011) 557–563.
[54] A.B. Afzal, M.J. Akhtar, M. Nadeem, M. Ahmad, M.M. Hassan, T. Yasin, M. Mehmood, Structural and electrical properties of polyaniline/silver nanocomposites, J. Phys. D. Appl. Phys. 42 (2009) 015411–015419.
[55] W. Xing, J. Cheng, Frontiers in Biochip Technology, 2006. 279.
[56] H.H.S. Javadi, F. Zuo, K.R. Cromack, M. Angelopoulos, A.G. Mac Diarmid, A.J. Epstein, Charge transport in the "emeraldine" form of polyaniline, Synth. Met. 29 (1989) 409–416.
[57] A.N. Papathanassiou, J. Grammatikakis, S. Sakkopoulos, E. Vitoratos, E. Dalas, Localized and long-distance charge hopping in fresh and thermally aged conductive copolymers of polypyrrole and polyaniline studied by combined TSDC and dc conductivity, J. Phys. Chem. Solids 63 (2002) 1771–1778.
[58] A.K. Jonscher, Dielectric Relaxation in Solids, Chelsea Dielectric Press, London, 1983.
[59] C. Shan, H. Yang, D. Han, Q. Zhang, A. Ivaska, L. Niu, Electrochemical determination of NADH and ethanol based on ionic liquid-functionalized graphene, Biosens. Bioelectron. 25 (2010) 1504–1508.

[60] L. Rotariu, O. Istrate, C. Bala, Poly(allylamine hydrochloride) modified screen-printed carbon electrode for sensitive and selective detection of NADH, Sensors Actuators B 191 (2014) 491–497.
[61] L. Li, H. Lu, L. Deng, A sensitive NADH and ethanol biosensor based on graphene–Au nanorods nanocomposites, Talanta 113 (2013) 1–6.
[62] J. Zeng, X. Gao, W. Wei, X. Zhai, J. Yin, L. Wu, X. Liu, K. Liu, S. Gong, Fabrication of carbon nanotubes/poly(1,2-diaminobenzene) nanoporous composite via multipulse chronoamperometric electropolymerization process and its electrocatalytic property toward oxidation of NADH, Sensors Actuators B 120 (2007) 595–602.
[63] D. Gligor, Y. Dilgin, I.C. Popescu, L. Gorton, Poly-phenothiazine derivative-modified glassy carbon electrode for NADH electrocatalytic oxidation, Electrochim. Acta 54 (2009) 3124–3128.
[64] M. Zhang, A. Smith, W. Gorski, Carbon nanotube-chitosan system for electrochemical sensing based on dehydrogenase enzymes, Anal. Chem. 76 (2004) 5045–5050.
[65] L. Zhu, R. Yang, X. Jiang, D. Yang, Amperometric determination of NADH at a Nile blue/ordered mesoporous carbon composite electrode, Electrochem. Commun. 11 (2009) 530–533.
[66] M. Musameh, J. Wang, A. Merkoci, Y. Lin, Low-potential stable NADH detection at carbon-nanotube-modified glassy carbon electrodes, Electrochem. Commun. 4 (2002) 743–746.
[67] M. Zhou, L. Shang, B. Li, L. Huang, S. Dong, The characteristics of highly ordered mesoporous carbons as electrode material for electrochemical sensing as compared with carbon nanotubes, Electrochem. Commun. 10 (2008) 859–863.
[68] M. Zhou, Y. Zhai, S. Dong, Electrochemical sensing and biosensing platform based on chemically reduced graphene oxide, Anal. Chem. 81 (2009) 5603–5613.
[69] M. Wooten, W. Gorski, Electrocatalysis of dihydronicotinamide adenosine diphosphate with quinones and modified quinone electrodes, Anal. Chem. 82 (2010) 1299–1304.
[70] K. Guo, K. Qian, S. Zhang, J. Kong, C. Yu, B. Liu, Bio-electrocatalysis of NADH and ethanol based on graphene sheets modified electrodes, Talanta 85 (2011) 1174–1179.
[71] P.N. Bartlett, P.R. Birkin, E.N.K. Wallace, Oxidation of β-nicotinamide adenine dinucleotide (NADH) at poly(aniline)-coated electrodes, J. Chem. Soc. Faraday Trans. 93 (10) (1997) 1951–1960.
[72] L. Svorc, J. Sockr, M. Rievaj, P. Tamcik, D. Bustin, Voltammetric determination of penicillin V in pharmaceutical formulations and human urine using a boron-doped diamond electrode, Bioelectrochemistry 88 (2012) 36–41.
[73] D. Harvey, Modern Analytical Chemistry, 1st ed., 2000.

D. Sangamithirai has MSc degree in Physics from University of Madras. She has secured 1st Rank in MSc and was awarded INSPIRE Fellowship by DST, Government of India. She is currently working on polymer nanocomposites and electrochemical sensors.

Dr. V. Narayanan (MSc, Ph.D.) did his postgraduate studies in Madurai Kamaraj University and was awarded Gold Medal. He did his Ph.D. in the University of Madras and currently working as an Associate Professor in the Department of Inorganic Chemistry, University of Madras. His area of specialization is bioinorganic chemistry, nanomaterials, catalysis, photochemistry, environmental chemistry, electrochemistry, sensors and solar cells.

Dr. B. Muthuraaman (MSc, Ph.D.) did his Ph.D. in the University of Madras. He is working as an Assistant Professor in the Department of Energy, University of Madras. He works on dye sensitized solar photovoltaics and polymer electrolytes.

Dr. A. Stephen (MSc, MPhil, Ph.D.) did his Ph.D. in the University of Madras. He was a ICTP-TRIL fellow funded by UNESCO and Italian Foreign Ministry, Italy (2006–07). He is currently working as an Associate Professor in the Department of Nuclear Physics, University of Madras. His research interest is electrodeposition, biosensors, magnetic nanomaterials, photocatalytic materials, nanocomposites and XRD.